International Journal of Biological Macromolecules 286 (2025) 138414

Contents lists available at ScienceDirect

International Journal of Biological Macromolecules

journal homepage: www.elsevier.com/locate/ijbiomac

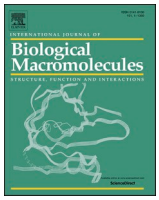

Cellulose-based underwater superoleophobic coatings with robust anti-viscous oil-fouling property for complex oily wastewater remediation

Xiaojing Su [a], Fawei Xie [a], Junlin Li [a], Yiyang Huang [a], Kunquan Li [a], Huali Xie [a], Wenjian Wu [a,*], Xin Xie [b,*]

[a] School of Materials Science and Engineering, Dongguan University of Technology, Dongguan 523808, China
[b] School of Pharmacy, Guangdong Medical University, Dongguan 523808, China

ARTICLE INFO

Keywords:
Underwater superoleophobicity
Anti-viscous oil-fouling
Durability
Crude oil/water separation
Heteromorphic cellulose crystal

ABSTRACT

Underwater superoleophobic coatings, known for their anti-oil-fouling properties, have garnered significant interest in the context of oily wastewater remediation. However, these coatings encounter challenges in preventing viscous oil contamination and structural damage, and easily become ineffective when treating crude oil/water pollutants. Additionally, the non-renewable and non-biodegradable components pose a huge risk to environmental safety and sustainable development. Herein, a cellulose-based coating that combines robust underwater superoleophobicity with anti-viscous oil-fouling characteristic is designed via the extraction of micro/nanoscale heteromorphic cellulose crystals (EHCC) and subsequent crosslinking with carboxymethyl chitosan (CCS). Leveraging the hierarchical micro/nanostructures constructed by EHCC and intensified hydration capability facilitated by multiple hydrogen bonding interactions, the EHCC-CCS coating demonstrates excellent superhydrophilicity/underwater superoleophobicity and ultralow-viscous oil-adhesion property. Moreover, the EHCC-CCS coating exhibits robust chemical resistance and mechanical tolerance. Importantly, it adapts effectively to various flat and porous substrates, offering outstanding anti-oil-fouling and self-cleaning performances. Notably, the EHCC-CCS-coated textile is applied in separating immiscible oil/water mixtures with varying oil viscosities, and the EHCC-CCS-coated PVDF membrane achieves to purify surfactant-stabilized crude oil/water emulsion. The findings provide a straightforward and cost-effective approach for large-scale production of fully biobased coatings with durable underwater superoleophobicity and excellent anti-viscous oil-fouling capability for complex oily wastewater remediation.

1. Introduction

Oily wastewater pollution originating from industrial sewage and crude oil leakage poses a significant threat to human health and ecological environment. In comparison to conventional techniques for oily wastewater remediation, membrane filtration has received burgeoning interest for the advantages of easy operation, high efficiency, and energy savings [1–3]. Specifically, membranes modified with hydrophilic/underwater superoleophobic coatings are popular, which strongly repel oil to prevent adhesion and further ensure stable oil/water separation [4–7]. Inspired by the self-cleaning property of fish scales in oily wastewater, constructing a hydrophilic/underwater superoleophobic coating involves hierarchical morphologies and intrinsically hydrophilic components [8,9]. The micro/nano rough structure of such a coating easily traps water to create a hydration layer, which is important to obstruct direct contact and adhesion of oil pollutants to the coating surface.

Oily wastewater remediation includes the removal of immiscible oil slicks from water and purification of oil/water emulsions. In recent years, a series of membranes with hydrophilic/underwater superoleophobic property have been developed for oily wastewater separation [10–13]. For example, Peng et al. [14] constructed an antibacterial nanocomposite membrane by vacuum-assisted filtration of the hydrothermally produced silver nanoparticles@tunicate cellulose nanocrystal suspension onto a support film. The membrane efficiently separated oil/water microemulsions with a water flux over than 324 $L{\cdot}m^{-2}{\cdot}h^{-1}{\cdot}bar^{-1}$ and oil rejection exceeding 99 %. Yang et al. [15] proposed a facile surface diffuse atmospheric plasma method to functionalize the nylon mesh with micro/nano composite structures, enabling large-area immiscible oil/water separation with an efficiency larger than 99.9 %

* Corresponding authors.
E-mail addresses: wuwj@dgut.edu.cn (W. Wu), xiexin@gdmu.edu.cn (X. Xie).

https://doi.org/10.1016/j.ijbiomac.2024.138414
Received 12 September 2024; Received in revised form 29 November 2024; Accepted 3 December 2024
Available online 7 December 2024

and intrusion pressure of ~3 kPa. However, the targeted oils by most hydrophilic/underwater superoleophobic membranes are low-viscosity oils and organic solvents. The viscous crude oil with complex composition and strong adhesion poses challenges in oil/water separation due to the serious membrane pollution [16,17]. This issue is particularly pronounced when dealing with surfactant-stabilized crude oil/water emulsions, resulting in membrane pore blockage and rapid decline in separation performance [18–20]. Unfortunately, there are limited reports to date on fabricating the hydrophilic/underwater superoleophobic coatings that can effectively resist the intrusion of viscous oil and achieve efficient crude oil/water remediation.

Theoretically, the stronger the hydration capability of the hydrophilic/underwater superoleophobic coatings, the better the barrier effect in forming a hydration layer and preventing oil fouling [21,22]. Accordingly, hydrogels, inorganic minerals, metal compounds and hydrophilic polymers have been proposed to modify the porous membranes, aiming to strengthen the hydration capability and achieve efficient crude oil/water separation [23–26]. For instance, Jiang et al. [27] employed synergistic segment orientation and covalent anchoring strategies to design underwater superoleophobic hydrogel coatings on various substrates, which demonstrated long-term antiswelling and antibiofouling properties for crude oil self-cleaning. Xiang et al. [28] developed a robust superhydrophilic/underwater superoleophobic PVA/GO@MOF membrane with a chemically crosslinkable structure, exhibiting extraordinary anti-oil adhesion for high-viscosity crude oil slick and emulsion purification. However, majority of the hydrophilic/underwater superoleophobic coatings rely on non-renewable and non-biodegradable inorganic micro/nanoparticles and petroleum derivatives, thus posing significant risks to environmental safety, recyclability and sustainable development. In contrast, cellulose and its derived micro/nanoscale materials have garnered interest in superwettable coatings due to their renewability, biodegradability, and ease of surface modification [29,30]. Nevertheless, challenges persist in achieving chemical/physical stability, substate adaptability and large-scale preparation of the hydrophilic/underwater superoleophobic coatings for practical application.

In this study, a fully organic underwater superoleophobic coating with robust anti-viscous oil-fouling property was fabricated by extracting the micro/nanoscale heteromorphic cellulose crystals from *Enteromorpha prolifera* (EHCC) and crosslinking them with carboxymethyl chitosan (CCS). By combining the hierarchical micro/nanostructures constructed by EHCC with strong hydration capability contributed to multiple hydrogen bonding interactions, the EHCC-CCS coating presented superhydrophilicity with a water contact angle (WCA) below 5^{o} within 10 s and underwater superoleophobicity with oil contact angles (OCAs) above 153^{o}. The EHCC-CCS coating exhibited an ultralow adhesion force to crude oil underwater of nearly 0 μN, and demonstrated high repellence toward viscous silicone oil with a viscosity of 20,000 mPa·s (25 °C). Importantly, the EHCC-CCS coating showed robust underwater superoleophobic stability to resist various chemical and physical damages. Moreover, the EHCC-CCS coating adapted well to various substrates (e.g., glass slide, iron sheet, textile, stainless-steel mesh, and PVDF membrane) with great anti-viscous oil-fouling and self-cleaning performances. Delightedly, the EHCC-CCS-coated textiles effectively removed immiscible oil slicks from water with high water collection efficiency and permeation flux, and the EHCC-CCS-coated PVDF membranes realized efficient surfactant-stabilized crude oil-in–water emulsion separation with remarkable oil rejection. Our findings highlight a straightforward and cost-efficient strategy to fabricate fully organic hydrophilic/underwater superoleophobic coatings with outstanding durability and anti-viscous oil-fouling property for complex oily wastewater remediation.

2. Experimental section

2.1. Materials

Enteromorpha prolifera (EP) was collected from the beaches of Qingdao (China). Carboxymethyl chitosan (CCS, deacetylation degree ≥90 %) was bought from Shanghai Macklin Reagent Co., Ltd. (China). Glutaraldehyde (GA, AR, 50 % in water), ethanol (AR), sodium hydroxide (NaOH, 96 %), sodium chlorite ($NaClO_2$, 80 %), and glacial acetic acid (AR, 36 %) were purchased from Aladdin Reagent Co., Ltd. (China). Hydrochloric acid (HCl, 36–38 %) and *n*-hexane (AR) were supplied by Guangzhou Chemical Reagent Factory (China). Crude oil (viscosity = 780 mPa·s at 25 °C) was obtained from Sinopec Maoming Petrochemical Co., Ltd. (China). Vegetable oil was got from the local market, and silicone oil (viscosity = 20,000 mPa·s at 25 °C) was provided by Shenzhen Jipeng Silicon Fluorine Material Co., Ltd. (China). All chemicals were used as received without further purification.

2.2. Extraction of micro/nanoscale heteromorphic cellulose crystals from EP

Cellulose crystals were extracted using a modified version of a previous work [31]. Firstly, the sun-dried EP was washed with water to remove sediment impurities, and then grounded into powdered form in an electric blender after oven drying. Next, 10 g of fine EP power was degreased through Soxhlet extraction with ethanol as solvent at 115 °C for 6 h. Subsequently, the degreased EP was dispersed in a buffer solution consisting of 10 mL of glacial acetic acid, 4 g of $NaClO_2$ and 200 mL of water, and then stirred at 65 °C for 6 h to destruct the cell walls and remove pigments from EP. After centrifugation and washing with water for several times, the obtained bleached EP was reacted in 200 mL of 0.5 M NaOH solution at 65 °C for 12 h to remove non-cellulose substances, and then underwent repeated water rinsing until the solution pH reached 7. Finally, the alkali treated sample was subjected to boiling HCl solution (5 wt%) for 20 min, and then kept stirring overnight at 35 °C to hydrolyze cellulose. After repetitive centrifugation and water washing, the sample was evenly dispersed in water via vigorous ultrasonic crushing to obtain the micro/nanoscale heteromorphic cellulose crystals (EHCC) dispersion with a concentration of 2 mg/mL.

2.3. Fabrication of underwater superoleophobic coatings on flat substrates

Briefly, CCS was dissolved in water to generate a CCS solution with a concentration of 2 mg/mL under magnetic stirring for 6 h. Subsequently, the EHCC and CCS solutions were mixed through an ultrasonic treatment for 15 min, and the EHCC/CCS mass ratio was controlled at x (x = 1, 2, 3, 4, and 5). Next, the glutaraldehyde was added and continuously stirred for 30 min to prepare a uniform EHCC/CCS dispersion, where the glutaraldehyde/CCS mass ratio was maintained at 10 wt%. For flat substrates including glass slide, polyethylene terephthalate (PET) film and iron plate, the EHCC/CCS dispersion was directly drop-coated on the oxygen plasma-treated surfaces, and then cured at 40 °C for 1 h to obtain the crosslinkable coating (denoted as EHCC-CCS-x).

2.4. Fabrication of underwater superoleophobic coatings on porous substrates

For porous substrates including textile, steel mesh and polyurethane (PU) sponge, the EHCC/CCS dispersion (x = 4) served as the modification liquid, and the detailed modification process proceeded as follows. An oxygen plasma-treated substrate was dipped into the EHCC/CCS dispersion, and then taken out and dried at 40 °C for 1 h. The dipping-drying process was repeated four cycles to produce a stable underwater superoleophobic porous substrate with desired EHCC-CCS loading. Additionally, to modify the polyvinylidene fluoride (PVDF) membrane, different volumes (0.5, 1, and 1.5 mL) of the EHCC/CCS dispersion (x =

4) were filtrated on the membrane, and then transferred into an oven at 40 °C for 1 h to obtain the EHCC-CCS-coated PVDF membrane.

2.5. Separation for immiscible oil/water mixtures

A piece of EHCC-CCS-coated textile was utilized as a filter membrane, securely positioned between two glass tubes to build a simple filtration device. Detailedly, low-viscosity *n*-hexane, medium-viscosity vegetable oil, and high-viscosity crude oil were selected as the representative oils. Next, the immiscible mixtures containing 20 mL of oil and 80 mL of water were poured into the device to achieve oil/water separation. The water collection efficiency was defined as the mass ratio of the separated water to that initially added into mixture. The permeation flux was calculated according to the following equation:

$$\text{Permeation flux} = \frac{V_1}{A_1 t_1} \quad (1)$$

where A_1 was the effective area of the EHCC-CCS-coated textile, and V_1 and t_1 represented the volume and separation time of oil/water mixture, respectively.

2.6. Separation for surfactant-stabilized oil-in-water emulsions

To thoroughly investigate the emulsion separation performance of the EHCC-CCS-coated PVDF membrane, oils with varying viscosities (including *n*-hexane, vegetable oil, and crude oil) were chosen for the study. The surfactant-stabilized *n*-hexane-in-water, vegetable oil-in-water, and crude oil-in-water emulsions were respectively prepared by violently ultrasonicating the mixture of oil (1 mL), water (99 mL), and sodium dodecyl sulfate (SDS, 0.025 g) for 1 h. To separate the oil-in-water emulsions, an EHCC-CCS-coated PVDF membrane was fixed within a filtration device for filtering, with a circulating water vacuum pump to provide pulling force. Next, 30 mL of the oil-in-water emulsions were poured into the device to achieve separation. The permeation flux was calculated according to the following equation:

$$\text{Permeation flux} = \frac{V}{AtP} \quad (2)$$

where A was the effective area of the EHCC-CCS-coated PVDF membrane, P represented the pressure provided by vacuum pump, and V and t were the volume and separation time of oil-in-water emulsion, respectively.

2.7. Characterizations

Microscopic morphologies were captured by a Sigma 500 scanning electron microscope (SEM, Carl Zeiss Jena, Germany) at 5 kV, and the accompanied X-Max 20 energy dispersion spectroscopy (EDS, Oxford Instruments, UK) was used to test elemental distributions at 10 kV. Chemical compositions were obtained from Escalab 250Xi X-ray photoelectron spectroscopy (XPS, Thermo Fisher, USA) with an Al Kα monochromatic X-ray source and Nicolet iS10 Fourier transform infrared spectroscopy (FT-IR, Thermo Fisher Scientific, USA) from 4000 to 500 cm^{-1} with a scanning time of 32. Surface roughness was evaluated using a Dimension Icon atomic force microscopy (AFM, Bruker, Germany) in tapping mode with a scanning rate of 0.977 Hz. X-ray diffraction (XRD) spectra were conducted on a diffractometer (Bruker D8 Advance, Germany) to test crystal structure with a scanning rate of 5 °/min at room temperature. Water contact angles (WCAs, 3 μL) and underwater oil contact angles (OCAs, 8 μL) were recorded on a SDC-200S CA meter (Dongguan Shengding Precision Instruments Co., Ltd., China). Underwater adhesion force of crude oil was carried out by an automatic tension gauge (JK99M1, Shanghai Zhongchen Digital Technology Equipment Co., Ltd) using 8 μL of crude oil as probe liquid. AMEX1000 EVOS XL core imaging system (Thermo Fisher Scientific, USA) was utilized to collect optical microscopy images of emulsion droplets. Oil contents in filtrates were measured on a total organic carbon analyzer (Aurora 1030 W, USA).

3. Results and discussion

As natural renewable resources, the EHCC was extracted from abandoned *Enteromorpha prolifera* to construct hierarchical roughness and provide abundant -OH groups to interact with water, and the CCS was derived from marine organisms to strengthen chemical and mechanical stability. Through a crosslinking reaction between EHCC and CCS, the underwater superoleophobic EHCC-CCS coating with anti-viscous oil-fouling property was obtained. The schematic illustration of the fabrication process is presented in Fig. 1.

3.1. Extraction and characterizations of the EHCC

The fabrication process of the EHCC involved several steps including *Soxhlet* extraction for degrease, $CH_3COOH/NaClO_2$ treatment for depigmentation, NaOH treatment to remove non-cellulose substances, and HCl hydrolysis and ultrasonic crushing to separate micro/nanoscale cellulose crystals (Fig. 2a). The obtained EHCC was uniformly and stably dispersed in water. The pristine EP exhibited continuous block-like structure without obvious micro/nanoscale particles (Fig. 2b, b_1). After depigmentation, the lignin in cell wall of the blenched EP was removed to eliminate pigments. The surface became rougher, while the overall appearance remained blocky (Fig. S1a, a_1). Besides, the alkali treated EP removed hemicellulose and proteins. The intramolecular and intermolecular hydrogen bonds of cellulose were largely weakened by swelling, leading to the formation of microcrystalline cellulose (Fig. S1b, b_1). After further HCl hydrolysis and ultrasonic separation, the EHCC presented a sheet-like structure with uneven sizes ranging in length from 400 nm to 3.5 μm and a thickness of <50 nm (Fig. 2c, c_1). Notably, the EHCC dried using different ways displayed similar morphologies of micro/nanoscale heteromorphic sheets (Fig. S1c-d_1). Compared with regular shapes, such an uneven morphology was more effective to create hierarchical roughness.

Compared with the XRD spectrum of EP, several peaks appeared in the EHCC at 17.7°, 22.1°, and 35.0°, corresponding to (110), (200), and (004) crystal planes of cellulose I crystal pattern, respectively (Fig. 2d) [32,33]. The strong diffraction peak at 22.1° illustrated the high crystallinity of EHCC prepared by acid hydrolysis. In the FT-IR spectrum of EP, several typical peaks were observed at 3300 cm^{-1} (O—H stretching), 2900 cm^{-1} (C—H stretching), 1635 cm^{-1} (bound H_2O), 1543 cm^{-1} (skeletal vibration of phenyl ring), 1410 cm^{-1} (C—H bending), 1211 cm^{-1} (C-O-C stretching in syringyl ring of lignin), 1015 cm^{-1} (C—O vibration of cellulose), and 845 cm^{-1} (C—H bond deformation out of plane of aromatic ring) [34]. Obviously, the EP consisted of cellulose, lignin and other chemicals. Comparatively, the peak intensities at 3300, 1635, 1543, 1211, and 845 cm^{-1} of the bleached EP were greatly weakened, illustrating that part of lignin in EP was removed. In the spectrum of the alkali treated EP, the lignin and hemicellulose were totally cleaned for the disappearance of the characteristic peaks at 1543, 1211, and 845 cm^{-1}. After HCl hydrolysis and ultrasonic crushing, the obtained EHCC presented a new peak at 903 cm^{-1}, ascribing to the oscillation of β-1,4-glycosidic linkage between the dehydrated glucose units of cellulose. Additionally, a peak appeared at 1705 cm^{-1}, which was probably attributed to the carboxylic acid groups in *D*-glucuronic acid of *Ulva* plants (Fig. 2e) [31]. The FT-IR results was consistent with the XPS analysis (Fig. S2), demonstrating the successful extraction of cellulose crystals from natural EP. As shown in Fig. 2f, the EHCC formed a uniform film on the filter membrane after filtration. Due to the intramolecular and intermolecular hydrogen bonds of cellulose, the EHCC film demonstrated a great flexibility with no obvious damages after repeated bending deformations, which provided practical feasibility for application in flexible polymer composite materials.

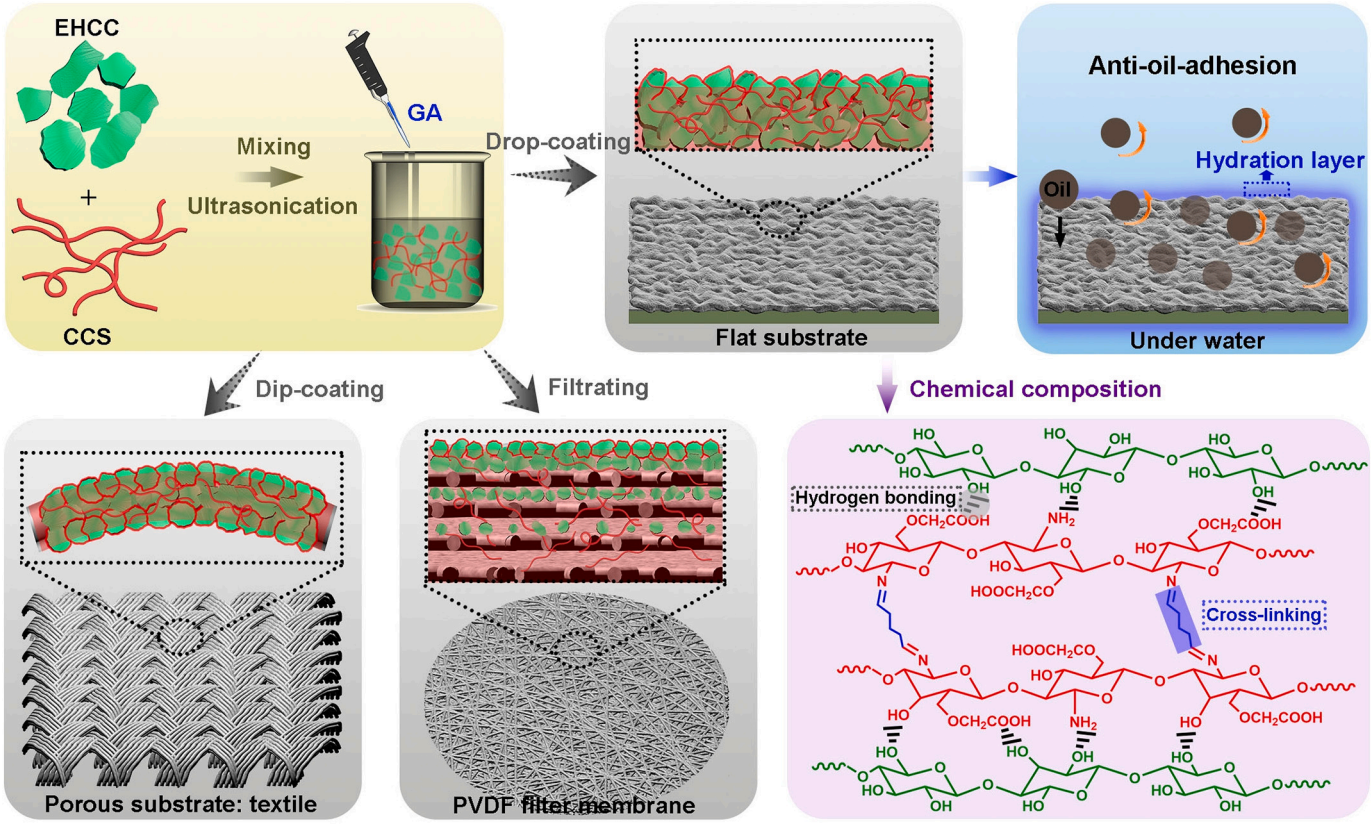

Fig. 1. Schematic diagram for fabricating the underwater superoleophobic EHCC-CCS coating.

3.2. Preparation and characterizations of the EHCC-CCS coatings on glass substrate

The superhydrophilic/underwater superoleophobic EHCC-CCS coating was constructed by incorporating EHCC to create micronano roughness and a cross-linkable structure with CCS to ensure stable hydrophilicity. Obviously, the EHCC-CCS mass ratio (*x*) greatly affected the microscopic morphology. When the *x* was 1 and 2, numerous microscale bulges were clearly observed on the EHCC-CCS coatings. However, due to the complete encapsulation of EHCC within CCS, constructing a nanoscale architecture was challenging for the high content of CCS (Fig. 3a-b$_1$). With the *x* increasing to 3 and 4, the EHCC contributed significantly to create nanosized roughness. This dense accumulation of EHCC led to the formation of protuberances on the EHCC-CCS coatings (Fig. 3c, c$_1$ and S3a, a$_1$). The resulting micronano morphology played a crucial role in achieving superhydrophilicity/underwater superoleophobicity. The coating surface exhibited uniform distribution of C, O, and N elements with atomic ratios of 67.2 %, 30.7 %, and 2.1 %, respectively (Fig. S3b, c). As the *x* rose to 5, the EHCC-CCS coating maintained a similar hierarchical structure, and the surface roughness was difficult to further improve (Fig. 3d, d$_1$).

AFM was adopted to demonstrate the 2D and 3D architectures of the EHCC-CCS coatings with the *x* at 1 and 4. Compared with the EHCC-CCS-1 coating with relatively flat surface and inapparent nanoscale roughness, the EHCC-CCS-4 coating presented hierarchical micro/nanostructures (Fig. 3e, f and S4). The roughness factor (*r*), a critical parameter to evaluate the coating roughness, was calculated according to the ratio of actual surface area to projected surface area [35]. The *r* of the EHCC-CCS-1 and EHCC-CCS-4 coatings were respectively 1.052 and 1.112, illustrating the increasing roughness with the improving EHCC/CCS mass ratio (Fig. S5a, b). Clearly, the AFM analyses were consistent with the SEM results.

The EHCC-CCS coating featured a multiple crosslinkable structure, in which the -NH_2 groups reacted with glutaraldehyde to form C═N bonds, and the functional groups such as -OH and -COOH interacted to generate hydrogen bonds. XPS and FT-IR were conducted to demonstrate the chemical composition of the EHCC-CCS-4 coating. The O 1 s, N 1 s, and C 1 s peaks were detected at 533, 399, and 286 eV, respectively (Fig. 3g). Detailedly, the C 1 s spectrum was deconvoluted at binding energies of 284.6, 285.4, 286.6, and 288.6 eV, belonging to C—C, C—N, C-O/C═N, and C═O bonds, respectively (Fig. 3h) [36]. Additionally, the N 1 s spectrum exhibited a C—N peak at 400.2 eV, a N—H peak at 399.5 eV, and a C═N peak at 398.6 eV, respectively (Fig. 3i) [37]. Compared with the FT-IR spectrum of CCS, a new peak appeared at 1645 cm^{-1} in the EHCC-CCS coating, corresponding to the stretching vibration of C═N bonds (Fig. S5c). The XPS and FT-IR results confirmed the Schiff base reaction between -NH_2 groups and glutaraldehyde [38,39]. The multiple crosslinkable structure with chemical bonds and hydrogen bonds endowed the EHCC-CCS coating with excellent underwater stability even after 7 days of storage (Fig. S6).

3.3. Underwater superoleophobic behavior of the EHCC-CCS coatings on glass substrate

To comprehensively evaluate the surface wettability of the EHCC-CCS coatings, the WCAs, underwater OCAs, and anti-viscous oil-adhesion behavior were measured. Fig. 4a presents the WCA optical images on the EHCC-CCS coatings with varying EHCC/CCS mass ratios (*x*). When water droplet came into contact with the coating surface, it quickly spread for the strong water affinity of hydrophilic groups and micronano roughness constructed by EHCC. Unfortunately, the EHCC-CCS-1 and EHCC-CCS-2 coatings failed to achieve superhydrophilicity with the WCAs at 28° and 17° at 10 s, respectively. Comparatively, the EHCC-CCS-3, EHCC-CCS-4, and EHCC-CCS-5 coatings demonstrated superhydrophilicity with the WCAs reaching 9°, 4°, and 0° at 10 s, respectively. Additionally, the EHCC-CCS coatings displayed an

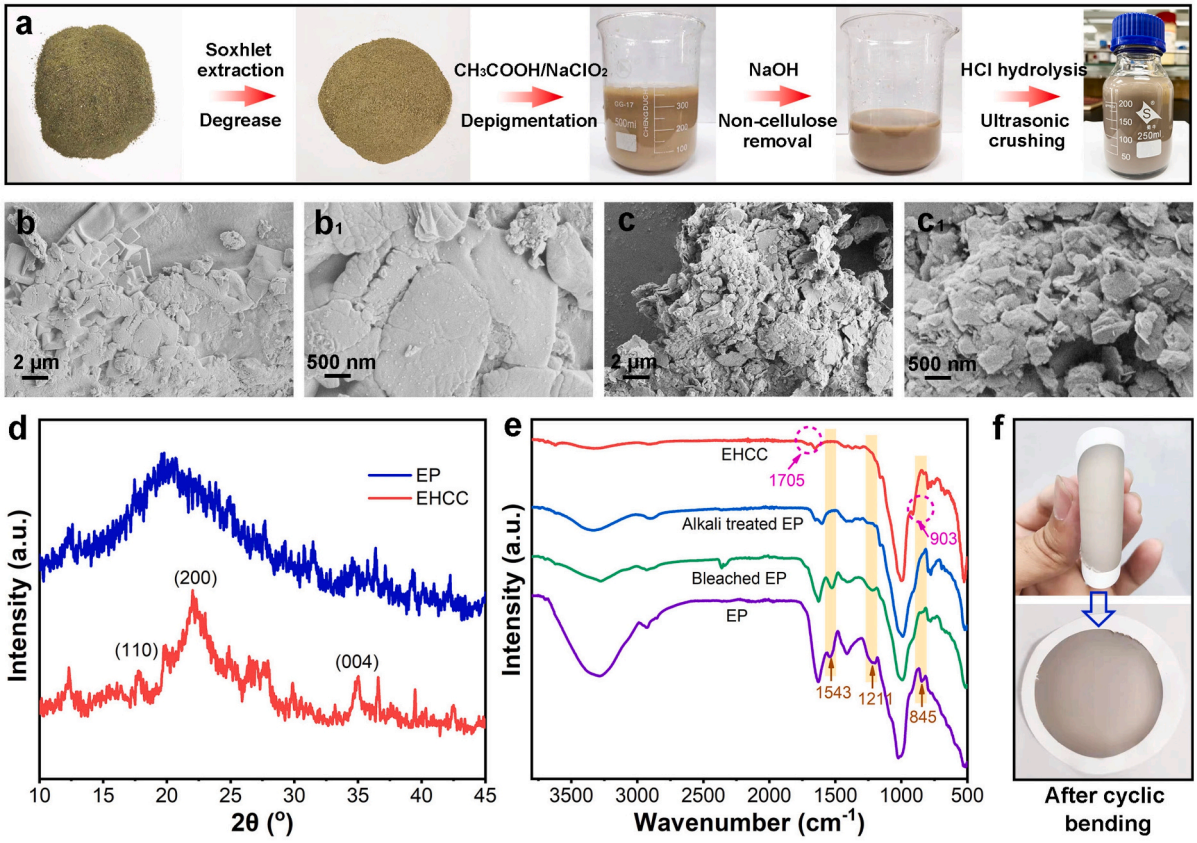

Fig. 2. (a) Fabrication process of the EHCC. SEM images of the (b, b_1) EP and (c, c_1) freeze-dried EHCC. (d) XRD patterns of the EP and EHCC. (e) FT-IR spectra of the EP, bleached EP, alkali treated EP, and EHCC.

outstanding repellency to viscous crude oil with the underwater OCAs at 152° for EHCC-CCS-1, 153° for EHCC-CCS-2, 154° for EHCC-CCS-3, 155° for EHCC-CCS-4, and 156° for EHCC-CCS-4 (Fig. 4b). With the increasing *x*, the roughness of the EHCC-CCS coatings gradually improved, thus enhancing the hydrophilicity and underwater oleophobicity. Notably, the underwater superoleophobic surfaces might not necessarily exhibit superhydrophilicity [40,41]. When the microscopic morphology of the EHCC-CCS coating was sufficiently rough, the hydrophilic groups rapidly captured water, forming a stable hydration layer both inside and outside the rough structure to achieve underwater superoleophobicity. Additionally, various oils with different viscosities and surface tensions were utilized to characterize the oil resistances. Delightedly, the EHCC-CCS-4 coating displayed the underwater OCAs larger than 150° for dichloromethane, hexane, mineral oil, kerosene, petroleum ether, toluene, silicone oil, machine oil, light crude oil, and vegetable oil (Fig. 4c). Moreover, the crude oil droplet easily rolled off the EHCC-CCS-4 coating at a tilting angle of ~3°, demonstrating the strong oil repellence (Fig. 4d).

To measure the anti-viscous oil-adhesion behavior of the EHCC-CCS coatings in aqueous environment, the crude oil (780 mPa·s at 25 °C) and silicone oil (20,000 mPa·s at 25 °C) were adopted to contaminate the coating surface. As shown in Fig. 4e and f, a crude oil droplet suspended on a ring and a dyed silicone oil droplet hanged on a dropper moved to contact the EHCC-CCS coating under water, and then were compelled to compress against the surface. When the oil droplet departed from the coating, no visible deformation was observed, and the adhesion force was nearly 0 μN (Fig. S7). The great capability to resist viscous oil adhesion arose from the pronounced hierarchical roughness of the EHCC-CCS coating constructed by the irregularly shaped EHCC particles at micro/nanoscale dimensions. Furthermore, the EHCC-CCS coating contained abundant functional groups including $-NH_2$, -OH and -COOH groups, which readily interacted with water to form multiple hydrogen bonds. Through the synergistic interplay of the physical morphology and chemical structure, the EHCC-CCS coating effectively entrapped water, forming a stable and robust hydration layer. Consequently, the highly viscous oil was difficult to break through the hydration layer to contact and pollute the EHCC-CCS coating even during the extrusion deformation process.

3.4. *Chemical and physical robustness of the underwater superoleophobic EHCC-CCS coatings*

The EHCC-CCS coating fabricated with *x* at 4 was selected for the following study. In practical terms, the chemical and physical robustness of the underwater superoleophobicity plays a crucial role in long-term application. To assess the pH stability of the EHCC-CCS coating, the samples were immersed into the aqueous solutions with varying pH values for 72 h (Fig. 5a). Remarkably, the EHCC-CCS coating maintained its underwater superoleophobicity within the pH range of 1 to 10, and the underwater crude oil CAs kept above 155° after acid/alkali treatment. Despite the highly viscous nature of silicone oil, it exhibited an ultralow adhesion to the treated EHCC-CCS coating at pH levels of 1 and 10. Notably, the EHCC-CCS coating kept excellent underwater superoleophobicity and anti-crude oil-fouling performance even after the immersion in acidic solution (pH = 1) for 15 days. However, exposure to solutions with a pH exceeding 11 for 12 h led to the lamination of the EHCC-CCS coating from the glass substrate (Fig. S8a). This susceptibility to strong alkalinity might result from the swelling damage caused by the $-NH_2$ groups of CCS reacting with NaOH [42]. Furthermore, immersion in NaCl solution (3.5 wt%) and SDS solution (1 g/L) for 72 h revealed that the EHCC-CCS coating displayed an underwater superoleophobicity and exceptionally low adhesive force toward silicone oil (Fig. S8b, c).

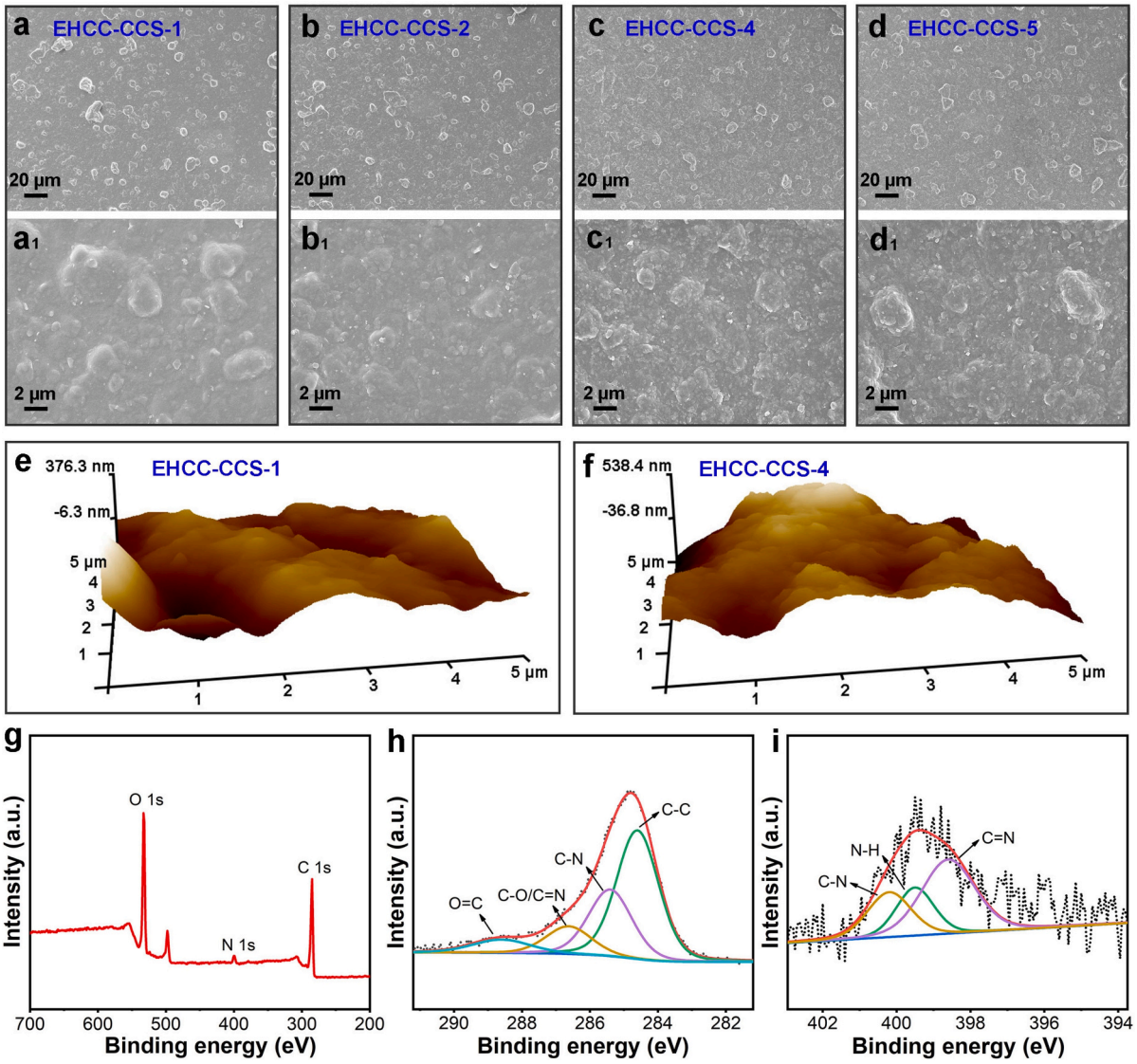

Fig. 3. SEM images of the (a, a_1) EHCC-CCS-1, (b, b_1) EHCC-CCS-2, (c, c_1) EHCC-CCS-4, and (d, d_1) EHCC-CCS-5 coatings. (e, f) AFM 3D surface structures of the EHCC-CCS-1 and EHCC-CCS-4 coatings. (g) XPS survey scan, (h) C 1 s spectra, and (i) N 1 s spectra of the EHCC-CCS-4 coating.

Additionally, following storage at temperatures of 10 and 80 °C for 72 h, the EHCC-CCS coating maintained the underwater crude oil CAs at 158° and 155°, respectively (Fig. 5b). Notably, no silicone oil residue was observed on the surface after being forced to sufficiently contact the treated coating (Fig. S8d, e). To assess the long-term stability, the EHCC-CCS coating was stored in ambient environment for 6 months. Throughout this period, the underwater crude oil CAs consistently remained above 155°, and the EHCC-CCS coating maintained its anti-silicone oil-adhesion performance after 6 months (Fig. 5c). The above results indicated the great chemical resistance of the EHCC-CCS coating, which mainly arose from the stable chemical structure formed through crosslinking via chemical and hydrogen bonding between EHCC and CCS.

The mechanical robustness of the underwater superoleophobicity of the EHCC-CCS coating was evaluated by the finger wipe, sandpaper abrasion, bending and water impact tests (Fig. 5d). After undergoing 200 cycles of finger wipe, the EHCC-CCS coating exhibited no significant changes in overall appearance. Under the function of the persistent micro-nano hierarchical structure of the EHCC, the underwater crude oil CA remained at 152° (Fig. 5e). When subjected to pressure from the high-viscosity silicone oil, the EHCC-CCS coating demonstrated excellent resistance to oil contamination (Fig. S9a). As for the sandpaper abrasion, the EHCC-CCS coating was abraded with a 2000 mesh sandpaper under a loading weight of 100 g (Fig. S9b). Noticeable scratches appeared on the coating surface after 40 cycles, while the overall micro-nano graded rough structure remained intact (Fig. 5f). The underwater crude oil CA of the treated EHCC-CCS coating maintained at 151°, and the silicone oil struggled to adhere to the scratched areas (Fig. S9c). Moreover, the water impact test was carried out using a water jet to attack the EHCC-CCS coating with water flow velocity of ~100 mL/min and vertical distance of ~19 cm (Fig. 5g). After impacting for 30 min, the EHCC-CCS coating remained underwater superoleophobicity and great anti-crude oil-adhesion performance (Fig. S9d). Furthermore, an EHCC-CCS coated PET film was respectively bent upward and downward to above 90° to measure the coating flexibility. After bending for 200 cycles, the underwater crude oil CA kept at 154°, and the coated film preserved excellent oil repellency (Fig. S9e, f). Notably, the EHCC-CCS coating presented excellent mechanical stability. On one hand, the multiple cross-linkable chemical structure formed by EHCC and CCS strengthened the bonding forces within the coating [4,43]. Thus, the EHCC was resistant to detachment under weak external forces. On the other hand, the high EHCC doping level ensured a consistently rough structure throughout the coating. Therefore, even if the severe external forces caused wear, the internal hierarchical roughness remains intact to

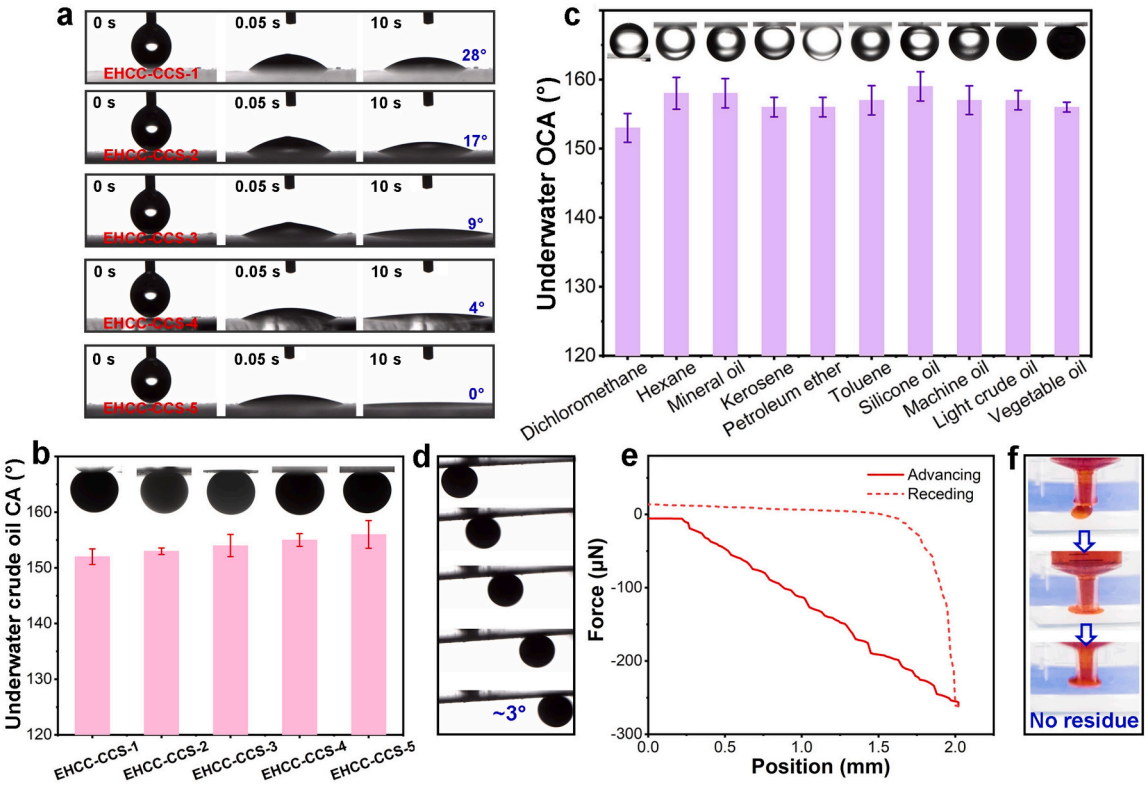

Fig. 4. (a, b) Spreading processes of water droplets and underwater crude oil CAs on the EHCC-CCS coatings fabricated with different *x*. (c) Underwater OCAs of various oils on the EHCC-CCS-4 coating. (d) Rolling process of crude oil on the underwater EHCC-CCS-4 coating. (e) Real-time force-distance curve during the dynamic crude oil-adhesion measurement on the EHCC-CCS-4 coating. (f) Underwater anti-silicone oil-adhesion process on the EHCC-CCS-4 coating.

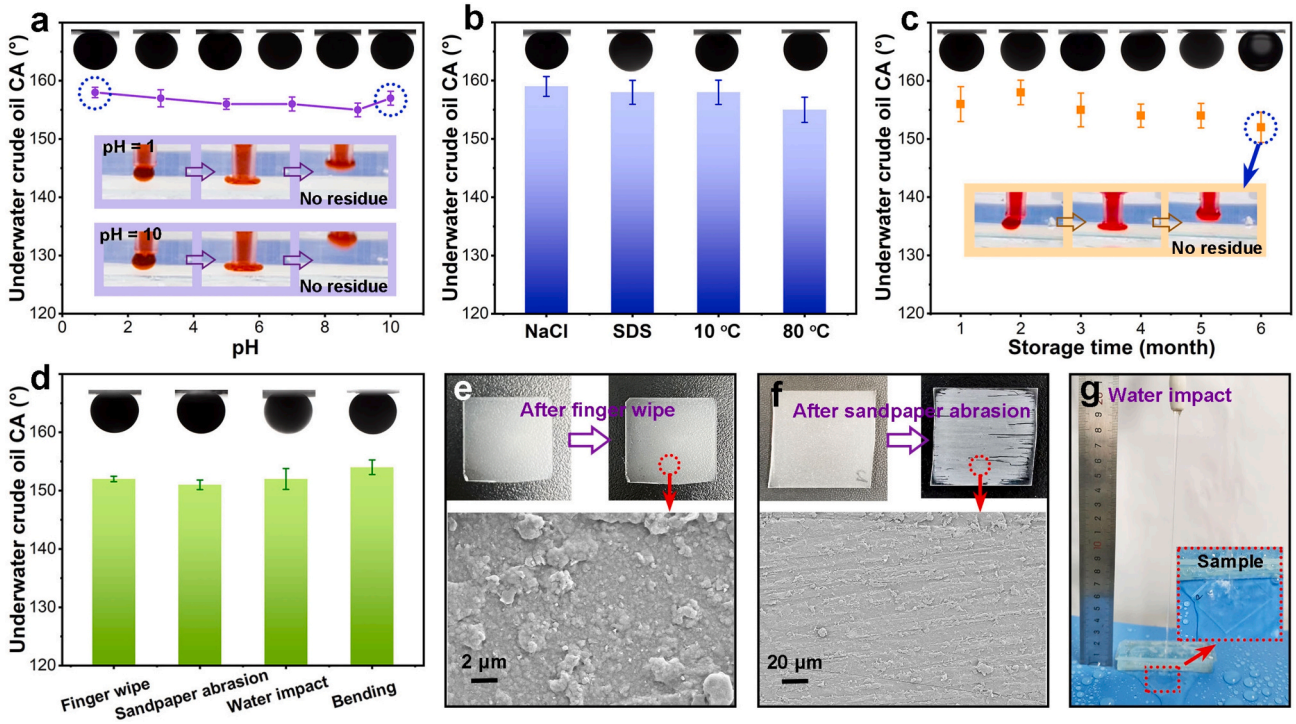

Fig. 5. Underwater crude oil CAs of the EHCC-CCS coatings after (a) treatment in water with pH from 1 to 10, (b) the immersion in NaCl and SDS solutions, and the storage at 10 and 80 °C for 72 h. (c, d) Changes of underwater crude oil CAs of the EHCC-CCS coatings with storage time and after mechanical damages. (e, f) Photographs and SEM images of the EHCC-CCS coatings after finger wipe and sandpaper abrasion tests. (g) Water impact test on the EHCC-CCS coating.

preserve the superwettability [26].

3.5. Adaptability of the EHCC-CCS coating on various porous substrates

In addition to the suitability for flat substrates, the EHCC-CCS coating was easily applied to porous substrates, including textile, stainless-steel mesh, and polyurethane sponge. Delightedly, the EHCC-CCS coating exhibited a strong affinity for the oxygen plasma-treated substrate surfaces, and provided a robust bonding force through chemical bonding and physical adsorption. The pristine cotton textile exhibited superhydrophilicity with a WCA at 0°, while the original stainless-steel mesh (400 and 80 meshes) and polyurethane (PU) sponge (density = 30 kg/m^3) were hydrophobic with the WCAs at 118°, 115°, and 123°, respectively. Comparatively, all the modified porous substrates transformed into a superhydrophilic state. The WCAs of the EHCC-CCS-coated textile, EHCC-CCS-coated steel mesh of 400 meshes, EHCC-CCS-coated steel mesh of 80 meshes, and EHCC-CCS-coated PU sponge rapidly decreased to 0° within 0.13, 0.27, 2.4, and 0.4 s, respectively (Fig. S10).

Delightedly, combining the roughness of the EHCC-CCS coating with the microscale skeleton of textile and steel mesh, the EHCC-CCS-coated textile and steel mesh (400 meshes) achieved underwater superoleophobicity with the crude oil CAs at 155° and 154°, respectively (Fig. 6a-b$_3$). Despite the severe deformation experienced by viscous crude oil and silicone oil, no obvious adhesion occurred, and the EHCC-CCS-coated textile and steel mesh (400 meshes) presented ultralow oil adhesion forces (Fig. S11a, b). The C, O, and N elements of the coated EHCC-CCS coating were evenly distributed on the skeleton of porous substrates (Fig. 6d-d$_3$). Comparatively, the underwater crude oil CAs of the pristine cotton textile and steel mesh (400 meshes) were only 148° and 100°, respectively, with apparent oil adhesion and residue observed on the uncoated surfaces (Fig. S11c, d). Unfortunately, due to the large holes in the steel mesh (80 meshes) and PU sponge, oil easily infiltrated these openings. Thus, the EHCC-CCS-coated steel mesh (80 meshes) and PU sponge exhibited low underwater crude oil CAs of 144° and 147°, respectively, with strong silicone oil adhesion occurring on the porous surfaces (Fig. 6c-c$_3$ and S12). Accordingly, the matched hierarchical structure created by the EHCC-CCS coating and porous skeleton played a crucial role in realizing underwater superoleophobicity and excellent anti-oil-adhesion performance [44].

3.6. Anti-oil-fouling behavior and immiscible oil/water separation of the EHCC-CCS-coated substrate

The anti-oil-fouling performance of the EHCC-CCS-coated substrates was investigated in relation to various oils. The dyed dichloromethane droplets presented sphere-like shape on the EHCC-CCS-coated iron plate. Upon jetting a riptide of dichloromethane onto the underwater EHCC-CCS-coated iron plate, numerous micro/nano droplets formed, forcefully bouncing off the superoleophobic surface. Notably, no oil droplets adhered to the plate (Fig. 7a). Furthermore, a patch of silicone oil was extruded onto the prewetted EHCC-CCS-coated steel mesh (400 meshes) in an air environment. When submerged in water, the silicone oil effortlessly levitated off the steel mesh without leaving any trace, while the oil on the untreated steel mesh remained firmly adhered (Fig. 7b). Additionally, a prewetted EHCC-CCS-coated textile experienced severe fouling by immersion in crude oil. However, upon immersion in water, the crude oil was promptly repelled, showcasing the excellent self-cleaning capability of the EHCC-CCS-coated textile. In contrast, the pristine textile only partially released the adhered crude oil

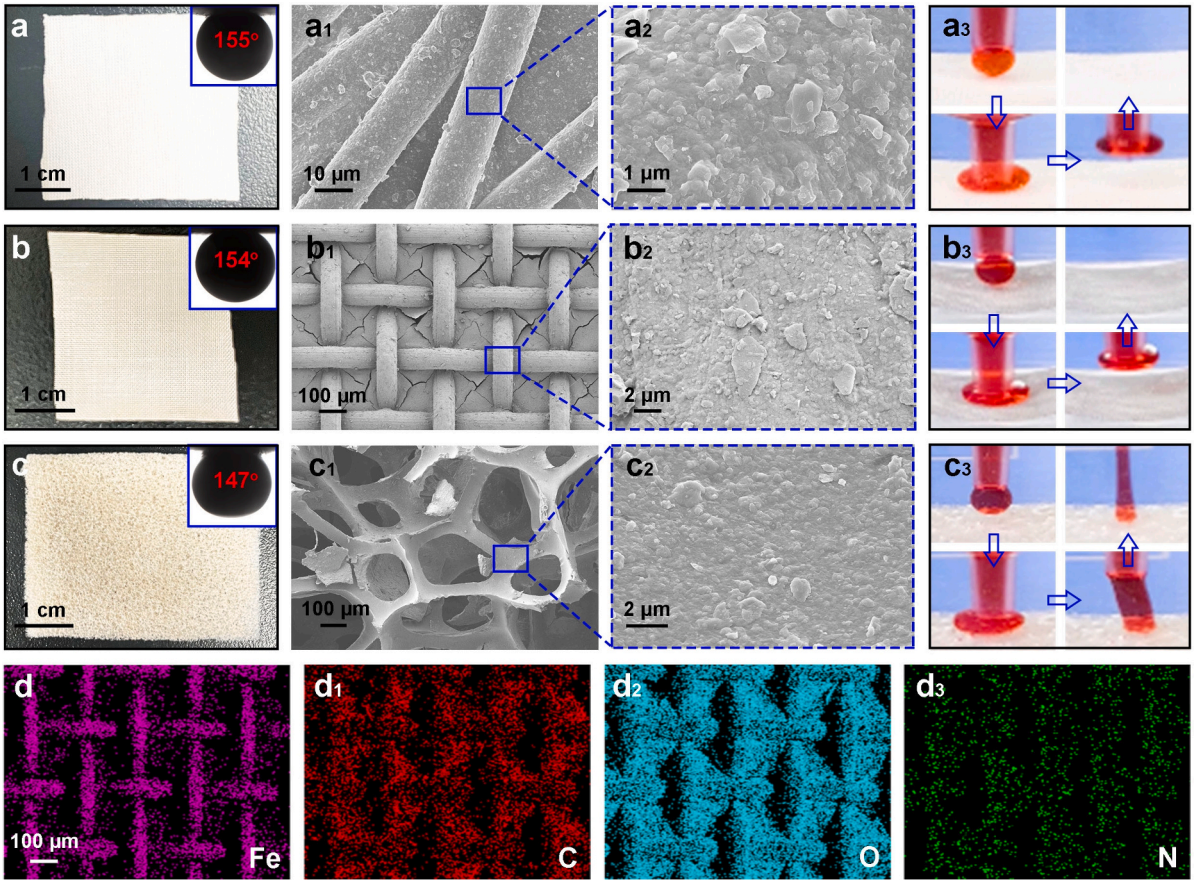

Fig. 6. Photographs, SEM images, and underwater anti-silicone oil-adhesion processes of the EHCC-CCS-coated (a-a$_3$) cotton textile, (b-b$_3$) steel mesh (400 meshes), and (c-c$_3$) PU sponge. (d-d$_3$) Mapping images of Fe, C, O, and N elements on the EHCC-CCS-coated steel mesh (400 meshes).

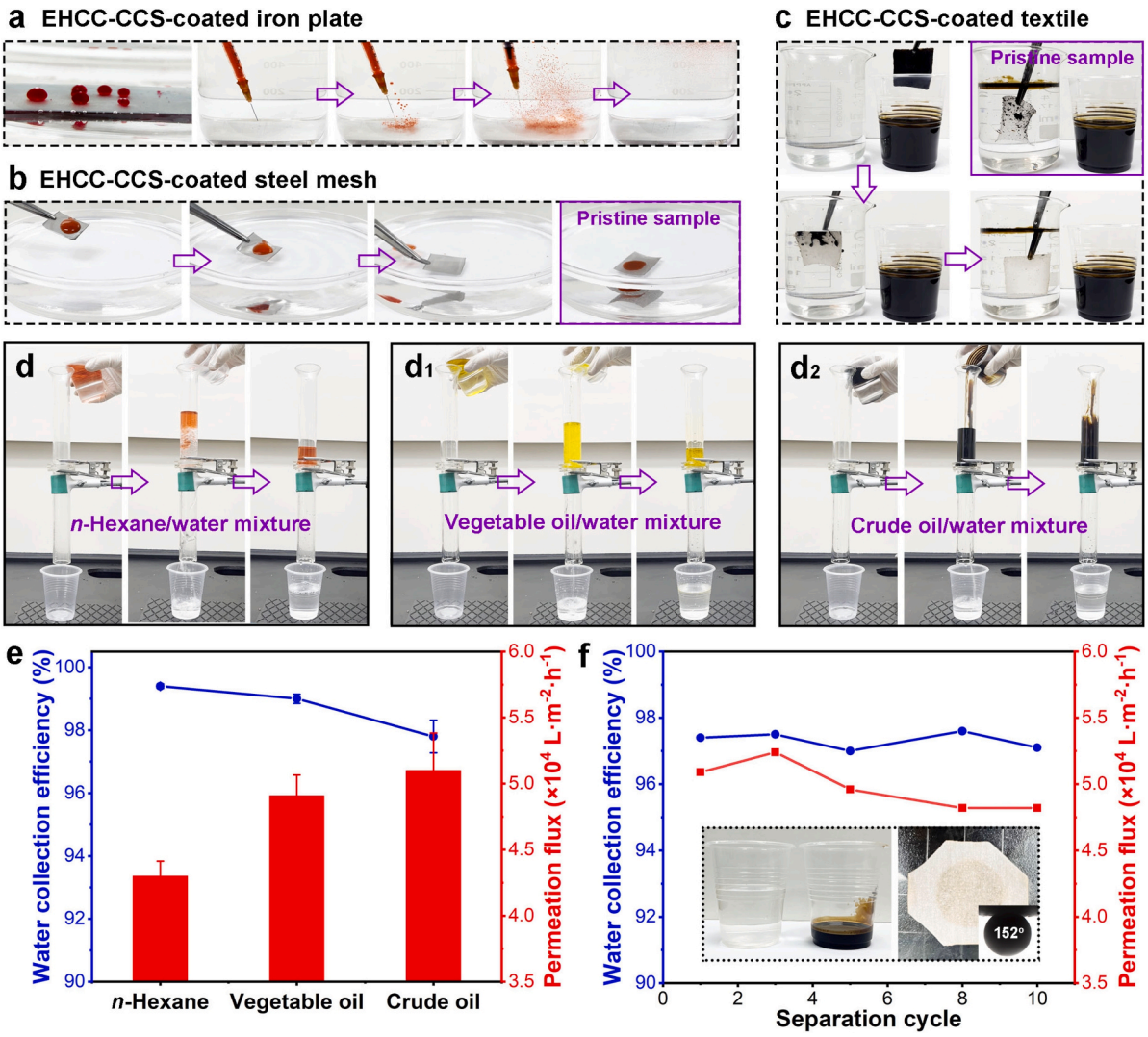

Fig. 7. (a) Underwater anti-dichloromethane-adhesion performance of the EHCC-CCS-coated iron plate. (b) Underwater anti-silicone oil-adhesion performance of the EHCC-CCS-coated steel mesh (400 meshes). (c) Underwater anti-crude oil-adhesion performance of the EHCC-CCS-coated textile. (d-d_2) Separation processes of *n*-hexane/water mixture, vegetable oil/water mixture, and crude oil/water mixture of the EHCC-CCS-coated textile. (e) Water collection efficiency and permeation flux of various immiscible oil/water mixtures. (f) Changes of crude oil/water separation performance with cycles.

(Fig. 7c). The exceptional anti-oil-fouling performance was attributed to the strongly and sufficiently hydrated layer that prevented oil adhesion on the EHCC-CCS-coated substrates in a water environment.

To assess the immiscible oil/water separation performance of the EHCC-CCS coating, the porous EHCC-CCS-coated textile was employed as a filtration membrane, and representative oily wastewater with various viscous oils (*n*-hexane/water, vegetable oil/water, and crude oil/water mixtures) was selected for evaluation. Under the influence of gravity, the water effortlessly permeated the EHCC-CCS-coated textile due to its superhydrophilicity and was collected in the beaker. Meanwhile, the oils were effectively rejected and remained on the textile surface due to its underwater superoleophobicity (Fig. 7d-d_2). Leveraging the hierarchical micro/nanostructures and intensified hydration capability facilitated by multiple hydrogen bonding interactions, the EHCC-CCS-coated textile successfully achieved to purify the immiscible oil/water mixture even with a high oil viscosity. Significantly, the water collection efficiencies for the *n*-hexane/water, vegetable oil/water, and crude oil/water mixtures highly reached 99.4 %, 99.0 %, and 97.8 %, respectively. The permeation fluxes presented a gradual increase with the higher oil viscosities, which were 4.3×10^4, 4.9×10^4, and 5.1×10^4 $L{\cdot}m^{-2}{\cdot}h^{-1}$ for *n*-hexane/water, vegetable oil/water, and crude oil/water mixtures, respectively (Fig. 7e). Evidently, the high-viscosity oil floating on water would force the water to passage across the EHCC-CCS-coated textile and promote the separation velocity. As a control experiment, the immiscible oil/water separation of the pristine textile was also measured. Except for the *n*-hexane/water mixture, the pristine textile failed to separate the vegetable oil/water and crude oil/water mixtures (Fig. S13). The weak and unstable hydration layer allowed the viscous vegetable oil and crude oil to displace water at surface and further penetrate the textile, resulting in serious membrane pollution and ineffective oil/water separation.

To further investigate the separation capability of the EHCC-CCS-coated textile, the intrusion pressures (*P*) of oils flowing through the textile were calculated ($P = \rho g h_{max}$, where ρ represented the oil density, *g* denoted the gravity acceleration, and h_{max} was the maximum height of oil that the EHCC-CCS-coated textile could support) [45]. The intrusion pressures presented a similar trend to the variation of permeation flux with viscosity (Fig. S14). Encouragingly, the intrusion pressures for the *n*-hexane, vegetable oil, and crude oil all exceeded 0.9 kPa, demonstrating the great oil resistance during the oil/water separation process. Additionally, the repeatability of the EHCC-CCS-coated textile for separating crude oil/water mixture was tested. After 10 of separation cycles, the crude oil/water mixture was still stably separated, and the water collection efficiency and permeation flux retained at 97.1 % and

4.82×10^4 $L{\cdot}m^{-2}{\cdot}h^{-1}$, respectively. Besides, the underwater crude oil CA remained stable at 152°, and no significant oil adhesion was observed on the EHCC-CCS-coated textile surface (Fig. 7f). Furthermore, the used EHCC-CCS-coated textile still kept the exceptional underwater superoleophobicity and anti-oil-fouling property after 100 cycles of sandpaper abrasion (Fig. S15). Thanks to the strong hydration layer, the EHCC-CCS-coated textile exhibited outstanding crude oil/water separation performance with high efficiency and reusability.

3.7. Oil-in-water emulsion separation of the EHCC-CCS-coated PVDF membrane

Practically, the purification of crude oil/water emulsion is difficult due to the emulsion stability and high viscosity of crude oil. To measure the separation performance of the EHCC-CCS-coating in crude oil-in-water emulsion, different volumes of the EHCC/CCS solution were filtrated on a commercial PVDF membrane to prepare an EHCC-CCS-coated PVDF membrane. Unlike the morphology of the original PVDF membrane, a large number of EHCC particles were clearly observed on the porous EHCC-CCS-coated PVDF membrane (Fig. 8a-a_2). As the volume of the EHCC/CCS solution increased, the EHCC-CCS coating on the PVDF membrane became significantly thicker and rougher, resulting in fewer pores and narrower pore channels (Fig. 8b-c_2). However, when the volume of the EHCC/CCS solution further improved to 1.5 mL, the porous structure was largely obstructed due to the sufficient incorporation of EHCC particles (Fig. 8d, d_1). The AFM images revealed the hierarchical micro/nanostructures of the EHCC-CCS-coated PVDF membrane fabricated with 1 mL of EHCC/CCS solution (Fig. 8e). The *r* reached 1.256, which was advantageous for resisting the attack and adhesion of highly viscous crude oil.

The commercial PVDF membrane exhibited a great superhydrophilicity with the WCA rapidly reaching 0° within 1.2 s. Despite the excellent water absorption capability, the PVDF membrane was susceptible to adhesion by viscous crude oil and silicone oil, and the underwater crude oil CA was only 139°. Due to the coverage of the EHCC-CCS coating, the porous EHCC-CCS-coated PVDF membrane demonstrated the improved water absorption time as the volume of the EHCC/CCS solution increased (Fig. 9a and S16). Specifically, the WCAs of the EHCC-CCS-coated PVDF membranes deceased to 0° within 1.4, 2.2, and 4.0 s for EHCC/CCS solution volumes at 0.5, 1, and 1.5 mL, respectively. Notably, the EHCC-CCS coating imparted excellent underwater superoleophobicity to the PVDF membrane, achieving the underwater crude oil CAs exceeding 155° (Fig. 9b). When the EHCC/CCS solution volume was 0.5 mL, the EHCC-CCS coating was too thin to fully cover the PVDF membrane, leading to the silicone oil fouling on the EHCC-CCS-coated PVDF membrane (Fig. S17a, b). However, at volumes of 1 and 1.5 mL, the EHCC-CCS-modified PVDF membranes exhibited minimal adhesion to crude oil and silicone oil, with an adhesion force close to 0 μN (Fig. 9c and S17c, d).

Three types of SDS-stabilized oil-in-water emulsions, composed of *n*-hexane, vegetable oil, and crude oil, were provided as examples to evaluate the emulsion separation performance of the EHCC-CCS-coated PVDF membranes (Fig. 9d). Initially, pure water filtration was conducted, and the obtained pure water fluxes decreased from 17,000 to 8060 $L{\cdot}m^{-2}{\cdot}h^{-1}{\cdot}bar^{-1}$ as the volume of the EHCC/CCS solution increased from 0 to 1.5 mL. Similarly, the permeation flux of the *n*-hexane-in-water emulsion displayed a reducing trend, ranging from 14,800 to 1100 $L{\cdot}m^{-2}{\cdot}h^{-1}{\cdot}bar^{-1}$. Clearly, the pore sizes and porosities of the filter membrane significantly influenced the separation velocity of the organic solvent-based emulsions. Accordingly, the pristine PVDF membrane demonstrated the optimal performance in separating the *n*-hexane-in-water emulsion. However, the changing trend of permeation fluxes differed markedly for the viscous vegetable oil-in-water and crude oil-in-water emulsions. With the EHCC/CCS solution volumes at 0, 0.5, 1, and 1.5 mL, the permeation fluxes for the vegetable oil-in-water emulsion were 203, 1120, 2285, and 724 $L{\cdot}m^{-2}{\cdot}h^{-1}{\cdot}bar^{-1}$, and the permeation fluxes for the crude oil-in-water emulsion were 12, 69, 159, and 185 $L{\cdot}m^{-2}{\cdot}h^{-1}{\cdot}bar^{-1}$, respectively. Obviously, the anti-oil-adhesion

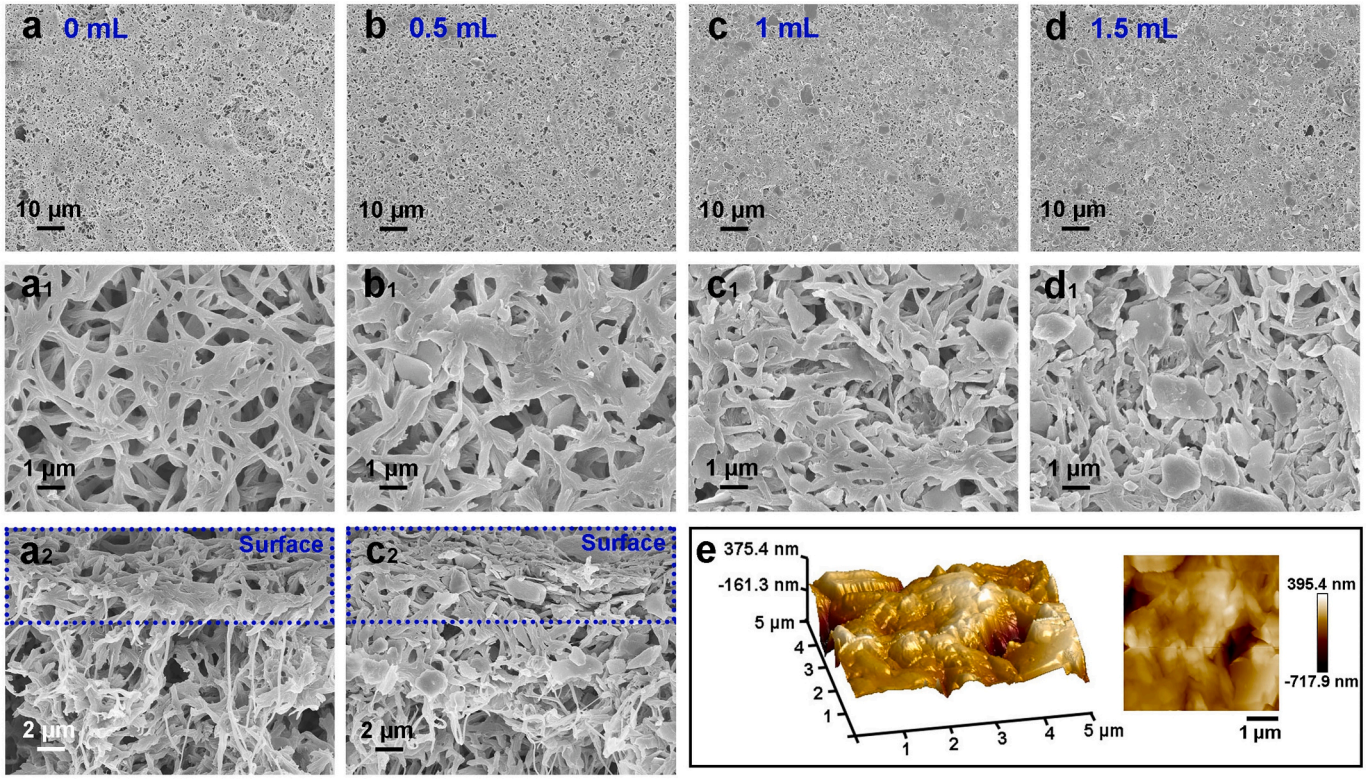

Fig. 8. SEM images of the EHCC-CCS-coated PVDF membrane fabricated with different EHCC/CCS solution volumes: (a-a_2) 0 mL, (b, b_1) 0.5 mL, (c-c_2) 1 mL, and (d, d_1) 1.5 mL. (e) AFM images of the EHCC-CCS-coated PVDF membrane fabricated with 1 mL of EHCC/CCS solution.

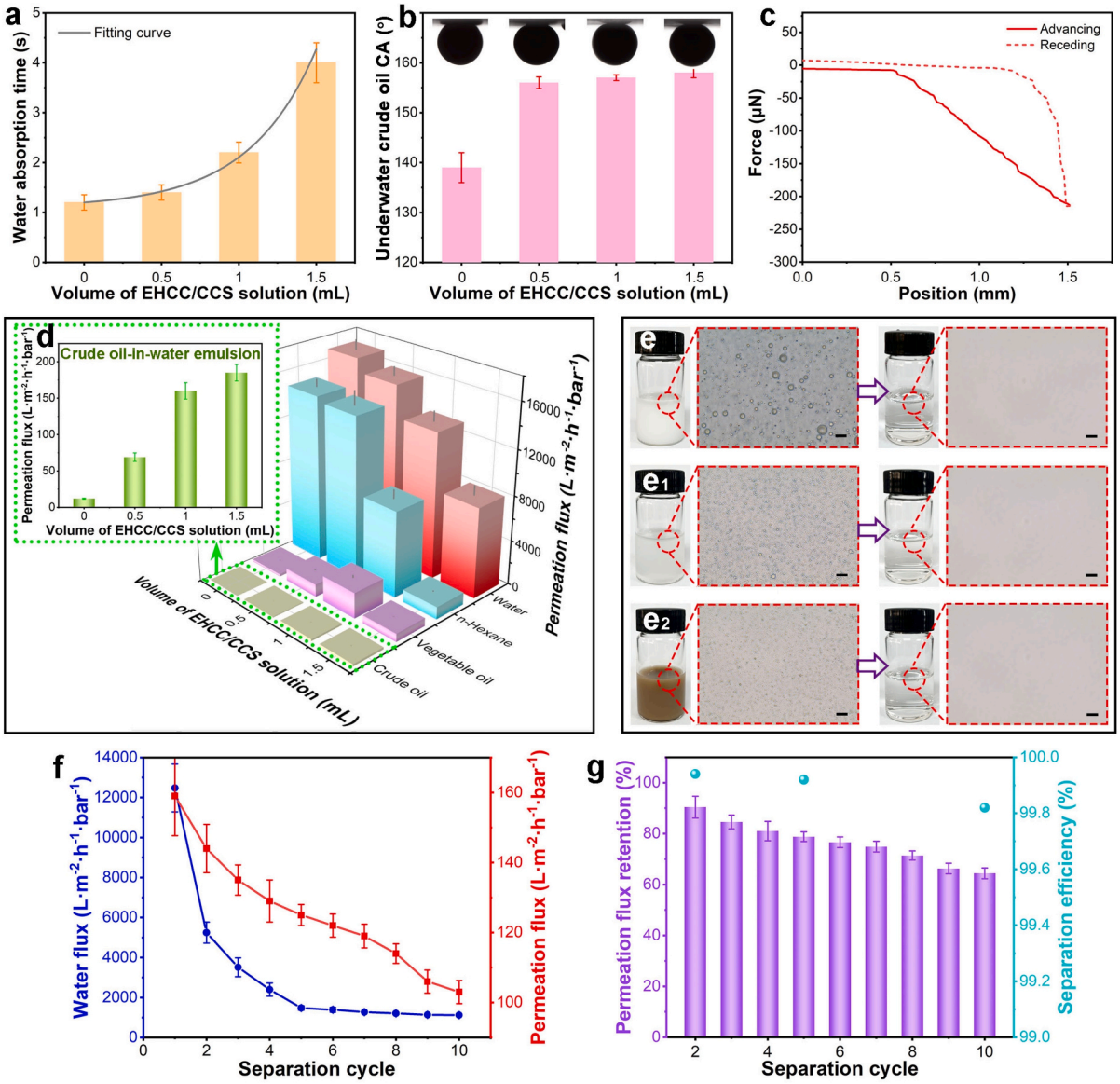

Fig. 9. (a, b) Water absorption time and underwater crude oil CAs of the EHCC-CCS-coated PVDF membranes. (c) Real-time force-distance curve during the dynamic crude oil-adhesion measurement on the EHCC-CCS-coated PVDF membrane fabricated with 1 mL of EHCC/CCS solution. (d) Permeation fluxes of various oil-in-water emulsions separated by the EHCC-CCS-coated PVDF membranes fabricated with different EHCC/CCS solution volumes. (e-e_2) Photographs and optical microscopy images of the *n*-hexane-in-water, vegetable oil-in-water, and crude oil-in-water emulsions before and after filtration. Scale bar in images: 20 μm. (f, g) Changes in separation performance of the crude oil-in-water emulsion with cycles.

performance played a crucial role in determining the separation velocity of viscous oil-in-water emulsions. The PVDF membrane experienced serious fouling by viscous oil, resulting in pore blockage and hindering water passage through the membrane. For the EHCC-CCS-coated PVDF membrane modified with 1 mL of EHCC/CCS solution, its strong hydration capability provided an excellent anti-viscous oil-fouling property (Fig. S17e). The combination of this hydration effect with the porous structure featuring suitable pore channels led to outstanding separation performance for treating the surfactant-stabilized viscous emulsions.

The SDS-stabilized *n*-hexane-in-water and vegetable oil-in-water emulsions appeared milky white, and the SDS-stabilized crude oil-in-water emulsion exhibited a murky brown color. Following filtration by the EHCC-CCS-coated PVDF membrane (using 1 mL of EHCC/CCS solution), all opaque emulsions became transparent and clear, and the existed micro/nanoscale oil droplets in emulsions disappeared in the corresponding filtrates (Fig. 9e-e_2). The ^{1}H NMR spectrum of the collected oil demonstrated the water was nearly removed from the surfactant-stabilized oil-in-water emulsion (Fig. S18). To test the cyclic performance of the EHCC-CCS-coated PVDF membrane, pure water and crude oil-in-water emulsion were sequentially filtered for each cycle. After 10 of repeated cycles, the water flux decreased from the original 12,477 $L{\cdot}m^{-2}{\cdot}h^{-1}{\cdot}bar^{-1}$ to 1124 $L{\cdot}m^{-2}{\cdot}h^{-1}{\cdot}bar^{-1}$. Additionally, the permeation flux for the emulsion reduced from the pristine 159 $L{\cdot}m^{-2}{\cdot}h^{-1}{\cdot}bar^{-1}$ to 103 $L{\cdot}m^{-2}{\cdot}h^{-1}{\cdot}bar^{-1}$ with a retention of 64.4 % (Fig. 9f). Importantly, the separation efficiencies were above 99.8 % during the repeated filtration processes (Fig. 9g). Despite the flux decline due to the irreversible fouling, the separation performance for the crude oil-in-water emulsion of the EHCC-CCS-coated PVDF membrane still outperformed that of the commercial PVDF membrane. Importantly, the EHCC-CCS coating presented good thermal stability below 200 °C even after the immersion in the surfactant-stabilized crude oil-in-water emulsion for 24 h (Fig. S19). Table S1 compares the chemical composition, superwettable stability, substrate adaptability,

and emulsion separation performance of the EHCC-CCS coating with other reported underwater superoleophobic materials in the literature. Consequently, the EHCC-CCS coating with excellent anti-viscous oil-fouling behavior holds great potential for separating stable oil-in-water emulsions.

4. Conclusions

In summary, we demonstrated a biobased coating with durable underwater superoleophobicity and excellent anti-viscous oil-fouling performance based on the hybrid of natural EHCC and CCS. Under the synergistic effect of hierarchical roughness and multiple hydrogen bonding interactions with water, the EHCC-CCS coating presented the strong hydration capability to achieve superhydrophilicity with a WCA of 4^{o} within 10 s, underwater superoleophobicity with a crude oil CA reaching 156^{o}, and ultralow adhesion force against viscous crude oil and silicone oil. Additionally, the EHCC-CCS coating behaved good superwettable stability to resist chemical and mechanical damages such as pH variations, temperature fluctuations, finger wipe, sandpaper abrasion, and water impact. Delightedly, the EHCC-CCS coating was versatile for various flat and porous substrates to enable superior superhydrophilicity/underwater superoleophobicity and anti-viscous oil-fouling performance. Furthermore, the EHCC-CCS-coated textile successfully separated the immiscible oil/water mixtures with varying oil viscosities, and the EHCC-CCS coated PVDF membrane realized the surfactant-stabilized crude oil-in-water emulsion separation with high efficiency, permeation flux, and reusability. The fabrication is simple, cost-effective, and available for large-scale production, and the green EHCC-CCS coating with durable underwater superoleophobicity and outstanding anti-viscous oil-fouling property represents a significant advancement for complex oily wastewater remediation.

CRediT authorship contribution statement

Xiaojing Su: Writing – original draft, Validation, Methodology, Investigation, Funding acquisition, Data curation. **Fawei Xie:** Methodology, Investigation, Data curation. **Junlin Li:** Validation, Investigation. **Yiyang Huang:** Methodology, Investigation. **Kunquan Li:** Formal analysis. **Huali Xie:** Conceptualization. **Wenjian Wu:** Visualization, Supervision, Funding acquisition. **Xin Xie:** Writing – review & editing, Resources, Methodology, Investigation.

Declaration of competing interest

The authors declare that they have no known competing financial interests or personal relationships that could have appeared to influence the work reported in this paper.

Acknowledgements

This study was supported by the National Natural Science Foundation of China (52203254), and the Guangdong Basic and Applied Basic Research Foundation, China (2023A1515140043, 2023A1515030056). XRD data were obtained using equipment maintained by the Analytical and Testing Center at Dongguan University of Technology.

Appendix A. Supplementary data

Supplementary data to this article can be found online at https://doi.org/10.1016/j.ijbiomac.2024.138414.

Data availability

Data will be made available on request.

References

[1] Y. Wang, S. Yang, J. Zhang, Z. Chen, B. Zhu, J. Li, S. Liang, Y. Bai, J. Xu, D. Rao, Scalable and switchable CO_2-responsive membranes with high wettability for separation of various oil/water systems, Nat. Commun. 14 (2023) 1108, https://doi.org/10.1038/s41467-023-36685-9.
[2] X. Yan, X. Xiao, C. Au, S. Mathur, L. Huang, Y. Wang, Z. Zhang, Z. Zhu, M.J. Kipper, J. Tang, Electrospinning nanofibers and nanomembranes for oil/water separation, J. Mater. Chem. A 9 (2021) 21659–21684, https://doi.org/10.1039/D1TA05873H.
[3] S. Zhang, X. Huang, D. Wang, W. Xiao, L. Huo, M. Zhao, L. Wang, J. Gao, Flexible and superhydrophobic composites with dual polymer nanofiber and carbon nanofiber network for high-performance chemical vapor sensing and oil/water separation, ACS Appl. Mater. Interfaces 12 (2020) 47076–47089, https://doi.org/10.1021/acsami.0c15110.
[4] X. Su, S. Huang, W. Wu, K. Li, H. Xie, Y. Wu, X. Zhang, X. Xie, Protonated cross-linkable nanocomposite coatings with outstanding underwater superoleophobic and anti-viscous oil-fouling properties for crude oil/water separation, J. Hazard. Mater. 436 (2022) 129129, https://doi.org/10.1016/j.jhazmat.2022.129129.
[5] H. Su, H. Hu, Z. Li, G. Yan, L. Wang, D. Xiang, C. Zhao, Y. Wu, J. Chen, C. Wang, Pre-oxidized PAN nanofibrous membrane to efficiently and continuously separate large-scale viscous oil-in-water emulsions under harsh conditions with ultra-long-term oil-fouling recovery, Adv. Fiber Mater. 6 (2024) 852–864, https://doi.org/10.1007/s42765-024-00383-y.
[6] S. Zhang, S. Chen, H. Li, X. Lai, X. Zeng, Superhydrophobic, flame-retardant and magnetic polyurethane sponge for oil-water separation, J. Environ. Chem. Eng. 10 (2022) 107580, https://doi.org/10.1016/j.jece.2022.107580.
[7] L. Liu, D. Yang, Y. Bai, X. Li, F.Z. Tan, J.L. Ma, Y.H. Wang, Construction of biodegradable superhydrophilic/underwater superoleophobic materials with CNF (cellulose nanofiber) fence-like attached on the surface for efficient oil/water emulsion separation, Int. J. Biol. Macromol. 269 (2024) 132175, https://doi.org/10.1016/j.ijbiomac.2024.132175.
[8] A. Borbora, R.L. Dupont, Y. Xu, X. Wang, U. Manna, Dually reactive multilayer coatings enable orthogonal manipulation of underwater superoleophobicity and oil adhesion via post-functionalization, Mater. Horiz. 9 (2022) 991–1001, https://doi.org/10.1039/D1MH01598B.
[9] H. Zhang, F. Wang, Z. Guo, The antifouling mechanism and application of bio-inspired superwetting surfaces with effective antifouling performance, Adv. Colloid Interfac. 325 (2024) 103097, https://doi.org/10.1016/j.cis.2024.103097.
[10] H. Du, F. Liu, H. Wang, Bio-inspired robust superhydrophilic/underwater superoleophobic coating with lubrication, anti-crude oil fouling and anti-corrosion performances, J. Colloid Interf. Sci. 616 (2022) 720–729, https://doi.org/10.1016/j.jcis.2022.02.090.
[11] S. Gan, H. Li, X. Zhu, X. Liu, K. Wei, L. Zhu, B. Wei, X. Luo, J. Zhang, Q. Xue, Constructing scalable membrane with tunable wettability by electrolysis-induced interface pH for oil–water separation, Adv. Funct. Mater. 33 (2023) 2305975, https://doi.org/10.1002/adfm.202305975.
[12] X. Zeng, J. Lin, W. Cai, Q. Lu, S. Fu, J. Li, X. Yan, X. Wen, C. Zhou, M. Zhang, Fabrication of superhydrophilic PVDF membranes by one-step modification with eco-friendly phytic acid and polyethyleneimine complex for oil-in-water emulsions separation, Chemosphere 264 (2021) 128395, https://doi.org/10.1016/j.chemosphere.2020.128395.
[13] J. Zhou, X. Li, T. Hou, X. Zhang, B. Yang, Biodegradable, biomimetic, and nanonet-engineered membranes enable high-flux and highly-efficient oil/water separation, J. Hazard. Mater. 434 (2022) 128858, https://doi.org/10.1016/j.jhazmat.2022.128858.
[14] K. Peng, Y. Huang, N. Peng, C. Chang, Antibacterial nanocellulose membranes coated with silver nanoparticles for oil/water emulsions separation, Carbohyd. Polym. 278 (2022) 118929, https://doi.org/10.1016/j.carbpol.2021.118929.
[15] L. Yang, Y. Feng, Z. He, X. Jiang, X. Luo, H. Dai, L. Jiang, Fast processing nylon mesh by surface diffuse atmospheric plasma for large-area oil/water separation, Nano Res. 16 (2023) 9625–9632, https://doi.org/10.1007/s12274-023-5677-z.
[16] Z. Chen, X. Su, W. Wu, J. Zhou, T. Wu, Y. Wu, H. Xie, K. Li, Superhydrophobic PDMS@GSH wood with joule heat and photothermal effect for viscous crude oil removal, Carbon 201 (2023) 577–586, https://doi.org/10.1016/j.carbon.2022.09.014.
[17] X.Y. Chen, M.Y. Yang, L.Y. An, J. He, K.R. Lai, Y.Y. Wang, A solar-driven nanocellulose Janus aerogel with excellent floating stability and dual functions of oil-water separation and photocatalytic degradation of organic pollutants, Int. J. Biol. Macromol. 278 (2024) 134698, https://doi.org/10.1016/j.ijbiomac.2024.134698.
[18] Q. Zhong, G. Shi, Q. Sun, P. Mu, J. Li, Robust PVA-GO-TiO_2 composite membrane for efficient separation oil-in-water emulsions with stable high flux, J. Membrane Sci. 640 (2021) 119836, https://doi.org/10.1016/j.memsci.2021.119836.
[19] Y.-L. Yang, G. Wang, P. Zhu, L. Tang, Z.-X. Zeng, L.-J. Zhu, In situ deposition of double Fe-based Fenton catalysts on the porous membrane for the development of multi-defense against various foulants toward highly efficient water purification, Chem. Eng. J. 471 (2023) 144498, https://doi.org/10.1016/j.cej.2023.144498.
[20] Y. Wang, Y. He, J. Yu, L. Zhang, S. Li, H. Li, Alginate-based nanofibrous membrane with robust photo-Fenton self-cleaning property for efficient crude oil/water emulsion separation, Sep. Purif. Technol. 287 (2022) 120569, https://doi.org/10.1016/j.seppur.2022.120569.
[21] J. Huang, J. Wu, J. Wu, D. Sun, Highly efficient separation for aqueous viscous oils enabled by a wood-based cellulose aerogel with a superhydrophilic protonated coating, ACS Sustain. Chem. Eng. 12 (2024) 7457–7465, https://doi.org/10.1021/acssuschemeng.4c00845.

[22] D.U. Lee, M. Kayumov, J. Park, S.K. Park, Y. Kang, Y. Ahn, W. Kim, S.H. Yoo, J.-K. Park, B.-G. Kim, Antibiofilm and antithrombotic hydrogel coating based on superhydrophilic zwitterionic carboxymethyl chitosan for blood-contacting devices, Bioact. Mater. 34 (2024) 112–124, https://doi.org/10.1016/j.bioactmat.2023.12.009.

[23] W. Chen, P. Zhang, S. Yu, R. Zang, L. Xu, S. Wang, B. Wang, J. Meng, Nacre-inspired underwater superoleophobic films with high transparency and mechanical robustness, Nat. Protoc. 17 (2022) 2647–2667, https://doi.org/10.1038/s41596-022-00725-3.

[24] A.-A. Adham, N. Kaixun, F. Duoxun, T. Zhengqiang, Fabrication of metal-based superhydrophilic and underwater superoleophobic surfaces by laser ablation and magnetron sputtering, Appl. Surf. Sci. 621 (2023) 156829, https://doi.org/10.1016/j.apsusc.2023.156829.

[25] R.-Y. Yue, P.-C. Yuan, C.-M. Zhang, Z.-H. Wan, S.-G. Wang, X. Sun, Robust self-cleaning membrane with superhydrophilicity and underwater superoleophobicity for oil-in-water separation, Chemosphere 330 (2023) 138706, https://doi.org/10.1016/j.chemosphere.2023.138706.

[26] H. Du, X. Zhao, X. Wang, C. Wang, Z. Liu, H. Wang, F. Liu, Surfactant-free emulsion of epoxy resin/sodium alginate for achieving robust underwater superoleophobic coating via a combination of phase separation and biomineralization, J. Colloid Interf. Sci. 642 (2023) 488–496, https://doi.org/10.1016/j.jcis.2023.03.166.

[27] X. Jiang, X. Xu, Z. Xia, D. Lin, Y. Chen, Y. Wang, D. Yu, X. Wu, H. Zeng, Simultaneous segment orientation and anchoring for robust hydrogel coating with underwater superoleophobicity, Adv. Funct. Mater. 34 (2024) 2314589, https://doi.org/10.1002/adfm.202314589.

[28] B. Xiang, J. Gong, Y. Sun, J. Li, Robust PVA/GO@MOF membrane with fast photothermal self-cleaning property for oily wastewater purification, J. Hazard. Mater. 462 (2024) 132803, https://doi.org/10.1016/j.jhazmat.2023.132803.

[29] Y. Zhu, H. Li, W. Huang, X. Lai, X. Zeng, Facile fabrication of superhydrophobic wood aerogel by vapor deposition method for oil-water separation, Surf. Interfaces 37 (2023) 102746, https://doi.org/10.1016/j.surfin.2023.102746.

[30] X.J. Su, W.H. Yang, K.Q. Li, H.L. Xie, Y.H. Wu, Y.F. Li, X. Xie, W.J. Wu, Fully organic and biodegradable superhydrophobic sponges derived from natural resources for efficient removal of oil from water, Sep. Purif. Technol. 277 (2021) 119411, https://doi.org/10.1016/j.seppur.2021.119411.

[31] K. Madub, N. Goonoo, F. Gimié, I.A. Arsa, H. Schönherr, A. Bhaw-Luximon, Green seaweeds ulvan-cellulose scaffolds enhance in vitro cell growth and in vivo angiogenesis for skin tissue engineering, Carbohyd. Polym. 251 (2021) 117025, https://doi.org/10.1016/j.carbpol.2020.117025.

[32] S. Naseem, A.I. Durrani, M. Rizwan, F. Yasmeen, S. Siddiqui, F. Habib, Sono-microwave assisted chlorine free and ionic liquid (SMACIL) extraction of cellulose from Urtica dioica: a benign to green approach, Int. J. Biol. Macromol. 259 (2024) 129059, https://doi.org/10.1016/j.ijbiomac.2023.129059.

[33] S. Nigam, A.K. Das, M.K. Patidar, Valorization of Parthenium hysterophorus weed for cellulose extraction and its application for bioplastic preparation, J. Environ. Chem. Eng. 9 (2021) 105424, https://doi.org/10.1016/j.jece.2021.105424.

[34] T. Gabriel, A. Belete, F. Syrowatka, R.H. Neubert, T. Gebre-Mariam, Extraction and characterization of celluloses from various plant byproducts, Int. J. Biol. Macromol. 158 (2020) 1248–1258, https://doi.org/10.1016/j.ijbiomac.2020.04.264.

[35] W. Weng, M. Tenjimbayashi, W.H. Hu, M. Naito, Evolution of and disparity among biomimetic superhydrophobic surfaces with gecko, petal, and lotus effect, Small 18 (2022) 2200349, https://doi.org/10.1002/smll.202200349.

[36] T.B. Taketa, J.B.M. Rocha Neto, D.M. Dos Santos, A. Fiamingo, M.M. Beppu, S. P. Campana-Filho, R.E. Cohen, M.F. Rubner, Tracking sulfonated polystyrene diffusion in a chitosan/carboxymethyl cellulose layer-by-layer film: exploring the internal architecture of nanocoatings, Langmuir 36 (2020) 4985–4994, https://doi.org/10.1021/acs.langmuir.0c00544.

[37] S.-S. Li, X.-L. Wang, Q.-D. An, Z.-Y. Xiao, S.-R. Zhai, L. Cui, Z.-C. Li, Upon designing carboxyl methylcellulose and chitosan-derived nanostructured sorbents for efficient removal of cd (II) and Cr (VI) from water, Int. J. Biol. Macromol. 143 (2020) 640–650, https://doi.org/10.1016/j.ijbiomac.2019.12.053.

[38] D. Zhang, L. Wang, H. Zeng, P. Yan, J. Nie, V.K. Sharma, C. Wang, A three-dimensional macroporous network structured chitosan/cellulose biocomposite sponge for rapid and selective removal of mercury (II) ions from aqueous solution, Chem. Eng. J. 363 (2019) 192–202, https://doi.org/10.1016/j.cej.2019.01.127.

[39] W. Yang, M. Pan, J. Zhang, L. Zhang, F. Lin, X. Liu, C. Huang, X.Z. Chen, J. Wang, B. Yan, A universal strategy for constructing robust and antifouling cellulose nanocrystal coating, Adv. Funct. Mater. 32 (2022) 2109989, https://doi.org/10.1002/adfm.202109989.

[40] R. Yue, M.S. Rahaman, Hydrophilic and underwater superoleophobic porous graphitic carbon nitride (g-C_3N_4) membranes with photo-Fenton self-cleaning ability for efficient oil/water separation, J. Colloid Interf. Sci. 608 (2022) 1960–1972, https://doi.org/10.1016/j.jcis.2021.10.162.

[41] B. Jiang, K. Cheng, N. Zhang, N. Yang, L. Zhang, Y. Sun, One-step modification of PVDF membrane with tannin-inspired highly hydrophilic and underwater superoleophobic coating for effective oil-in-water emulsion separation, Sep. Purif. Technol. 255 (2021) 117724, https://doi.org/10.1016/j.seppur.2020.117724.

[42] G. Ru, S. Wu, X. Yan, B. Liu, P. Gong, L. Wang, J. Feng, Inverse solubility of chitin/chitosan in aqueous alkali solvents at low temperature, Carbohyd. Polym. 206 (2019) 487–492, https://doi.org/10.1016/j.carbpol.2018.11.016.

[43] Y. Zhao, Y. Zhang, F. Li, Y. Bai, Y. Pan, J. Ma, S. Zhang, L. Shao, Ultra-robust superwetting hierarchical membranes constructed by coordination complex networks for oily water treatment, J. Membrane Sci. 627 (2021) 119234, https://doi.org/10.1016/j.memsci.2021.119234.

[44] C. Ma, L. Zhu, X. Qiao, H. Li, X. Zhu, J. Xue, Q. Xue, Ni-doped brochantite@copper hydroxide hierarchical structures on copper mesh with ultrahigh oil-resistance for high-efficiency oil/water separation, Surf. Coat. Technol. 406 (2021) 126642, https://doi.org/10.1016/j.surfcoat.2020.126642.

[45] L. Yang, Y. Feng, Z. He, X. Jiang, X. Luo, H. Dai, L. Jiang, Fast processing nylon mesh by surface diffuse atmospheric plasma for large-area oil/water separation, Nano Res. 16 (2023) 9625–9632, https://doi.org/10.1007/s12274-023-5677-z.